Original article

Institution of MECHANICAL ENGINEERS
Journal of MATERIALS: DESIGN AND APPLICATIONS

Proc IMechE Part L:
J Materials: Design and Applications
1–12

DOI: 10.1177/14644207211070965
journals.sagepub.com/home/pil
SAGE

Thermo-mechanical modelling of the Friction Stir Spot Welding process: Effect of the friction models on the heat generation mechanisms

Nasra Hannachi[1,2,3], Ali Khalfallah[1,4,5], Carlos Leitão[5,6] and Dulce Rodrigues[3]

Abstract

Friction Stir Spot Welding involves complex physical phenomena, which are very difficult to probe experimentally. In this regard, the numerical simulation may play a key role to gain insight into this complex thermo-mechanical process. It is often used to mimic specific experimental conditions to forecast outputs that may be substantial to analyse and elucidate the mechanisms behind the Friction Stir Spot Welding process. This welding technique uses frictional heat generated by a rotating tool to join materials. The heat generation mechanisms are governed by a combination of sliding and sticking contact conditions. In the numerical simulation, these contact conditions are thoroughly dependent on the used friction model. Hence, a successful prediction of the process relies on the appropriate selection of the contact model and parameters. This work aims to identify the pros and cons of different friction models in modelling combined sliding-sticking conditions. A three-dimensional coupled thermo-mechanical FE model, based on a Coupled Eulerian-Lagrangian formulation, was developed. Different friction models are adopted to simulate the Friction Stir Spot Welding of the AA6082-T6 aluminium alloy. For these friction models, the temperature evolution, the heat generation, and the plastic deformation were analysed and compared with experimental results. It was realized that numerical analysis of Friction Stir Spot Welding can be effective and reliable as long as the interfacial friction characteristics are properly modelled. This approach may be used to guide the contact modelling strategy for the simulation of the Friction Stir Spot Welding process and its derivatives.

Keywords

Friction Stir Spot Welding (FSSW), friction models, Finite Element Method (FEM), Coupled Eulerian-Lagrangian formulation (CEL), heat generation mechanisms

Date received: 8 September 2021; accepted: 15 December 2021

Introduction

Friction Stir Spot Welding (FSSW) is a solid-state spot welding technique derived from the linear Friction Stir Welding (FSW) process. This joining technique was developed and implemented by Mazda Motor Corporation in 1993 as an alternative to single-point joining methods such as Resistance Spot Welding (RSW).[1] Currently, despite being the most widely used welding process for vehicle structural assemblies, RSW may imply metallurgical issues associated with solidification for lightweight structural materials, like aluminium alloys.[2] FSSW process has received particular attention from both scientific and industrial communities. In this welding technique, the welds are created by plunging a rotating tool, into two overlapping plates, which are softened by frictional heating and joined by plastic deformation.[3] Due to plastic deformation, FSSW has the potential to produce high-strength joints.[4] However, the physics behind the process is still not thoroughly understood, since it involves coupled thermo-mechanical phenomena.

[1]Laboratoire de Génie Mécanique, Ecole Nationale d'Ingénieurs de Monastir, Université de Monastir, Monastir, Tunisia
[2]Ecole Nationale d'Ingénieurs de Sousse, Université de Sousse, Sousse, Tunisia
[3]Department of Mechanical Engineering, ISISE, University of Coimbra, Coimbra, Portugal
[4]Institut Supérieur des Sciences Appliquées et de Technologie de Sousse, Sousse, Tunisia
[5]Department of Mechanical Engineering, CEMMPRE, University of Coimbra, Coimbra, Portugal
[6]Department of Mechanical Engineering, ISEL, Polytechnic Institute of Lisbon, Lisbon, Portugal

Corresponding author:
Nasra Hannachi, Ecole Nationale d'Ingénieurs de Sousse, Université de Sousse, BP 264 Sousse Erriadh, 4023 Sousse, Tunisia.
Email: nasra.hannachi@gmail.com

Scarce published research works were addressing the analysis of the heat generation mechanisms and their relationship with the temperature evolution during welding. The analysis of heat generation was based on the conventional Coulomb law to describe the friction phenomenon at the tool-workpiece interface. The main reason for the scarcity of reports on such a subject is the complexity of the involved phenomena, which are very difficult to be experimentally probed. However, owing to the improvement of the computer power, researchers have developed numerical models to analyse the heat generation in FSSW. Finite Element Method (FEM) has been used for the numerical simulation of FSSW since about two decades ago. Several numerical analyses have been carried out in this respect and a wide range of numerical models were developed.

Muci-Küchler et al.[5] developed a 3D numerical model to simulate the isothermal plunge phase of the FSSW process. They focussed on the analysis of the flow stresses and the plastic deformation during welding. However, no thermal phenomena were analysed. Afterward, miscellaneous coupled thermo-mechanical models were developed to gain more insight into the fundamentals of the FSSW process.[6–8] Those models were used to predict the stress fields, the plastic deformation, and the temperature distribution during welding. They were based on some simplifications that limited an efficient analysis of such a complex FSSW process. The comparison between the numerical models outputs and experimental results, such as temperature, torque, force, etc., was presented without any analysis of the thermo-mechanical phenomena involved during the welding process. Therefore, the reliability of numerical modelling is still a debateable topic.

Based on the abovementioned literature survey, it is likely to state that a successful FSSW numerical simulation could be established based on an appropriate selection of the FE formulation, of a reliable constitutive material model, and of a friction model. In literature, special attention has been paid to the selection of the appropriate numerical formulation.[9–12] The combination of Lagrangian and Eulerian formulations was demonstrated to be the most effective for modelling the friction stir welding (FSW) process and its variants. On the other hand, the selection of the most appropriate material model for FSW is still limited. Generally, standard empirical models, such as Johnson Cook[8,13,14] and Norton-Hoff[15–17] constitutive models, are frequently used. Besides, the conventional Coulomb's law was used in the majority of FSSW numerical simulations. This friction law includes one coefficient of friction (COF) which is assumed as a constant value along the entire contact interface. Several values of COF were proposed for steel-aluminium pairs. Frigaard et al.[18] and D'Urso et al.[19] considered a COF of 0.4 as an average value from results in literature that reported on the FSW of AA6082-T6 aluminium alloy. Yang et al.[20] used a COF of 0.577 in the numerical simulation of the FSSW of the AA2198-T8 aluminium alloy; but, no argument was given on how this value was determined. Likewise, Bagheri et al.[14] assumed a COF of 0.35 for modelling the friction during the FSSW of AA5083 aluminium alloy.

In the abovementioned works, the evolution of temperature and the material flow during FSSW process were presented. However, none of them addressed the influence of the contact at the tool-workpiece interface on the output results. The contact conditions at the tool-workpiece interface are dependent on the local temperature and stress fields. Recently, Sanjeev et al.[11] and Chen et al.[8] established a modified version of Coulomb's law in which the limit shear stress of the welded material was introduced to control the stick-slip behaviour. In these works, the axial force, as well as the thermal history near the contact zone, were assessed. The obtained numerical results showed a good agreement with experimental ones. Scarce studies have used temperature-dependent COF for modelling the contact during welding. Khosa et al.[21] employed a temperature-dependent friction coefficient determined using an inverse approach. They developed a 2D numerical model to simulate the FSSW of AA6082-T6 aluminium alloy and a comparison with experimental results was performed. They reported that the thermal prediction was satisfactory. On the other hand, Meyghani et al.[22] developed a mathematical formulation to calculate the temperature-dependent friction coefficient during the FSW of AA6061-T6 aluminium alloy. This formulation was assessed with various rotational speeds and showed its capability to predict the peak temperature.

To date, only few analyses were achieved on the performance of different friction models on the simulation results of the FSSW process. Zhang et al.[23] compared the classical Coulomb's law and its modified version in modelling FSW of AA6061-T6 aluminium alloy. The authors considered a limit shear stress at the contact interface between the tool and the workpiece. They found for high rotational speed that the modified Coulomb law was more efficient in the FSW simulation. Dialami et al.[24] developed a modified version of Norton's law implemented in COMET[25] a dedicated FSW software. They took into account the sliding velocity and the pressure distribution at the tool-base material interface for modelling the contact conditions in the FSW of AA6063-T6 aluminium alloy. They compared Norton's law and its modified version predictions and they showed that the modified Norton's law has a great potential to reproduce experimental results. However, it is worth mentioning that in such cases, usually the agreement between numerical and experimental results was based on trial and error parameter fitting of the model. Therefore, the study of the effect of friction models on the outputs predicted by numerical simulation was not dealt with thoroughly and it is of great necessity. The lack of reports in this field consists the main motivation of the current work.

This work puts forward a fundamental basis for understanding the effect of friction models on temperature evolution and heat generation mechanisms during the FSSW

of the AA6082-T6 aluminium alloy. A three-dimensional (3D) coupled thermo-mechanical model using a coupled Eulerian-Lagrangian (CEL) approach was developed under ABAQUS/Explicit software. For a large range of temperatures, experimental stress-strain curves were used to describe the base material behaviour during FSSW process. Three friction models were adopted, namely: the conventional Coulomb friction model (CLB), the modified Coulomb model (MDF-CLB), and the temperature-dependent friction coefficient-based model (COF(T)) in the numerical simulation of FSSW. These friction models were chosen to study their effect on the heat generation mechanisms in the FE analysis of FSSW process. Particularly, their effect on the temperature evolution and both frictional and plastic energy dissipation was discussed. The findings of this investigation are helpful for directing the selection of the most appropriate friction model used for the FSSW simulation. The validation of the developed model was carried out by comparing predicted results with those obtained experimentally.

Thermo-mechanical modelling

Geometry, mesh, and numerical formulation

The numerical simulations were performed using ABAQUS/Explicit Finite Element code, which is well-established for handling non-linear problems. A fully coupled thermo-mechanical FE model was developed using the Coupled Eulerian-Lagrangian (CEL) approach. CEL formulation enables to selectively mesh the different model components, i.e. parts of the bodies undergoing large deformations are modelled using the Eulerian formulation, while the remaining are modelled using the conventional Lagrangian formulation.

Figure 1 shows the built CEL model, i.e. the partitions (a), the dimensions (b), and the mesh topology (c). For saving computation time, only the central part ($100 \times 100 \times 10$ mm) of the experimental samples was modelled. Moreover, to accurately capture differences in heat affected zones, a single rectangular sheet with a thickness of 10 mm substituted the two plates lap-welded. A similar procedure was used in the experimental tests. The idea of substituting the two lap plates with a single plate was based on Costa et al.[26] research work. It was stated that since the two plates are in very tight contact during lap joining, the heat distribution is uniform through the two plates thickness. A 10 mm diameter pinless cylindrical tool was used in this investigation.

The pinless tool was modelled as a rigid Lagrangian body and meshed with 13,271 four-node thermally coupled elements (C3D4T). The workpiece was modelled as an Eulerian domain, meshed with 58,240 multi-material thermally coupled 8-node Eulerian bricks. A refined mesh was assigned to the workpiece through the thickness direction (4 mm) to enhance the accuracy of the computation near the contact interface. As shown in Figure 1, a fictious layer was placed on the top of the Eulerian domain, which was created for enabling the visualization of any material motion outside the workpiece upper face. No constitutive properties were assigned

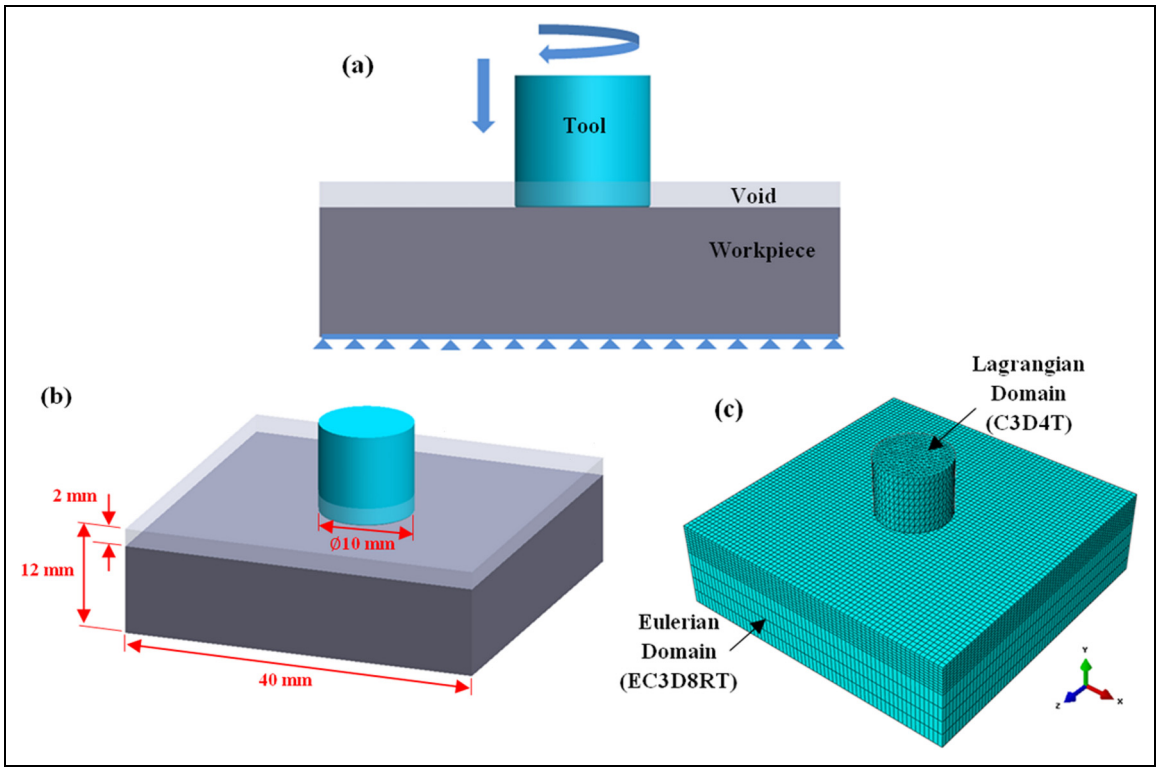

Figure 1. The model description: (a) CEL model partitions; (b) part dimensions; (c) mesh topology.

to this top layer. The size of this domain was chosen to prevent any outside material flow, which would become invisible during the ABAQUS post-processing. The material flow visualization was based on the output variable Eulerian Volume Fraction (EVF).[27] An EVF equal to one indicates that the mesh element is completely filled with the workpiece material, while an EVF of zero indicates that the element is empty (void). The computational time required for performing each analysis is about 69 h on a 2.80 GHz Intel® Xeon® processor.

Material behaviour

In order to accurately describe the material behaviour in FSSW, the material model should take into account the temperature and strain-rate dependency. In the present research work, the AA6082-T6 aluminium alloy, a heat-treatable (precipitation-hardened) aluminium alloy, was used as base material. This alloy is frequently used in welding construction and well-characterised in previous research works from current co-authors. Typically, the mechanical properties of the AA6082-T6 aluminium alloy exhibit a significant decrease during welding, due to the dissolution of the strengthening precipitates (β family).[28] In fact, starting at temperature 100 °C, the precipitates exhibit further growth (overaging) that weakens the precipitate-dislocation interaction, which induces the decrease of the yield strength. This material behaviour should be considered in the FSSW process simulation. Hence, a thermo-elastic-plastic material behaviour was adopted for the current simulations. Stress-strain data points, for different temperature values, were introduced in the property module of ABAQUS/Explicit. The input data were extracted from the stress-strain curves presented in Figure 2. These curves were obtained from the experimental results reported by Leitão et al.[29] and Summers et al.[30] According to Chen et al.[8] the strain rate has a minor impact on the flow stress and fracture behaviour of this AA6082-T6 aluminium alloy; therefore, its effect was neglected in the material modelling.

Contact modelling

The main objective of this paper is to use three friction models in the FSSW simulation and to assess their ability in the description of the inherent thermo-mechanisms during welding. These models are as follows:

- The conventional Coulomb model (CLB) which assumes that the critical shear stress at the tool-workpiece interface is proportional to the applied normal stress,[31] and expressed as

$$\tau_{crit} = \mu\sigma_N \tag{1}$$

where τ_{crit} is the frictional shear stress, σ_N is the normal stress and μ is the COF. This coefficient is constant along the contact surface during the simulation.[32] In this work, a constant COF value of 0.3 was selected according to different works on the modelling of FSW of 6xxx aluminium alloys using the classical Coulomb law.[33–35]
- The modified Coulomb model (MDF-CLB), in which two different critical shear stresses may be defined: the first one is given by equation (1), which is active when the contact shear stress is still lower than the yield shear stress of the material (τ_{yield}), the second one is given by

$$\tau_{crit} = \tau_{yield} \tag{2}$$

which is active when the contact shear stress reaches the yield shear stress of the base material. The yield shear stress of the material is estimated to be

$$\tau_{yield} = (\sigma_{yield} / \sqrt{3}), \tag{3}$$

where σ_{yield} is the base material initial yield stress. Using ABAQUS© software, only a constant value of the critical shear stress could be introduced in the Interaction module. Therefore, in the current analysis, the τ_{yield} adopted for the MDF-CLB model was an average value calculated using all the values of (σ_{yield}) presented in Figure 2. Hence, the critical shear stress is expressed as follows:

$$\tau_{crit} = min(\mu\sigma_N, \tau_{yield}). \tag{4}$$

The temperature-dependent friction coefficient-based model (COF(T)). According to this model, the critical shear stress is defined as

$$\tau_{crit} = \mu(T)\sigma_N, \tag{5}$$

where μ(T) is the temperature-dependent COF. The values of μ(T) used in the current analysis are given in Table 1.[22]

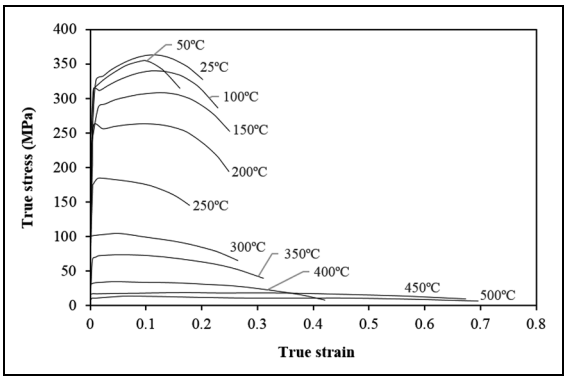

Figure 2. Base material behaviour at different temperatures.

Boundary conditions

In the current model, both thermal and mechanical boundary conditions are introduced. The thermal boundary conditions were assigned by prescribing an initial ambient temperature to both the tool and the workpiece. The heat transfer between the workpiece and the surrounding air was simplified using a convection coefficient of 30 W/m^{2}C. Thermal conductance was set to the contact

Table 1. Evolution of friction coefficient with temperature.[22]

Coefficient of friction	Temperature (°C)
0.25	25
0.23	50
0.20	100
0.19	150
0.18	200
0.15	250
0.10	300
0.05	350
0.025	400
0.015	450
0.010	500

Table 2. Thermal and mechanical properties of the workpiece and the tool materials.

	AA6082-T6 (workpiece)	H13 steel (tool)
Young's modulus; E (GPa)	70	210
Poisson's ratio; υ	0.33	0.1
Yield strength (MPa)	325	1650
Ultimate tensile strength (MPa)	385	1990
Elongation at break (%)	10	–
Density; ρ (Kg/m^3)	2700	7800
Conductivity; K (W/mC)	90	25
Expansion coefficient; α (C^{-1})	$21{,}1.10^{-6}$	$12{,}6.10^{-6}$
Specific heat; Cp (J/KgC)	900	500

interface between the tool and the workpiece. Depending on the contact pressure, two values of contact conductance were defined: 5000 W/m^{2}C, for the high-pressure conditions developed during the plunge and the dwell of the tool, and 1000 W/m^{2}C, for the low-pressure conditions developed during the retraction.[36] Thermal properties, such as conductivity, specific heat, and thermal expansion were also included in the 3D FE models (Table 2). In addition to the parameters above mentioned, a fraction of 0.9 was used to define the amount of heat generation associated with plastic deformation. For the tool-workpiece contact, it was assumed that 80% of the frictional heat was dissipated into the workpiece. For the mechanical boundary conditions, a plunge rate of 0.0417 m/s, and a rotational speed of 600 rpm were prescribed for the tool. The plunge depth was set equal to 0.5 mm. To represent the fixture and clamping system, the bottom and lateral surfaces of the workpiece were constrained; so that no lateral movement was allowed.

Experimental set up

Experimental spot welding was performed by plunging a pinless rotating tool into the workpiece, until reaching a predefined depth (position control), and then maintaining the tool at the same position, for a dwell period of 60 s. The tool used in these experiments was made of H13 steel. The material properties of the tool and the workpiece are listed in Table 2. In order to compare numerical results to those obtained in experiments, the same rotational speed (600 rpm) and plunge depth (0.5 mm) of the numerical simulations were used in the experimental tests. During the welding operation, the temperature evolution was registered using a thermographic camera, following the procedures explained by Andrade et al.[37] After welding, cross-sections were prepared by cutting across the centre of the welds to identify the different Process Affected Zones (PAZ). Standard techniques were used in preparing the metallographic samples for optical microscopy.

Numerical results and discussion

Temperature distribution

Figure 3 compares the temperature distribution obtained with the different friction models, during the plunge, the dwell, and the retraction stages. By examining the different graphs, it can be observed that the size of the high-temperature zone and its evolution along with the welding time are changed by varying the friction model. When using the CLB model, the temperature increases during the plunging and spreads throughout the contact interface to reach a maximum value of 300 °C at the start of the dwell period. However, before the end of the dwell period, a significant decrease in the maximum temperature occurs. On the other hand, when using the MDF-CLB model or the COF(T) based model, the highest temperature region does not spread to the entire contact interface and the peak temperature continuously increases until the end of the dwelling stage. Moreover, compared to the CLB model, it can be clearly seen that lower peak temperatures were computed, i.e. 250 °C using the MDF-CLB model and 225 °C using the COF(T) based model. At the beginning of the retraction, independently of the friction model, temperatures exhibit a gradual decrease, as a result of the convective heat transfer between the plate and the surrounding area.

Figure 4 displays a close-up view of the temperature distribution calculated at the end of the dwelling stage for the three friction models. The experimental weld micrograph was given for comparison purposes. Analysing the figure, it is obvious to observe that the highest temperature region was concentrated at the contact interface between the tool and the workpiece. For better lucidity, the contour of this region was overlaid with the PAZ (dashed line). Its shape and size coincide well with the PAZ region shown in the micrograph, particularly for the MDF-CLB and COF(T) based models. Both predicted temperature distribution and experimental cross-section weld present a W-shape contour. Similar findings concerning the temperature distribution and weld micrograph were reported by Yang et al.[20] The temperature distribution in the weld zone is a result of the

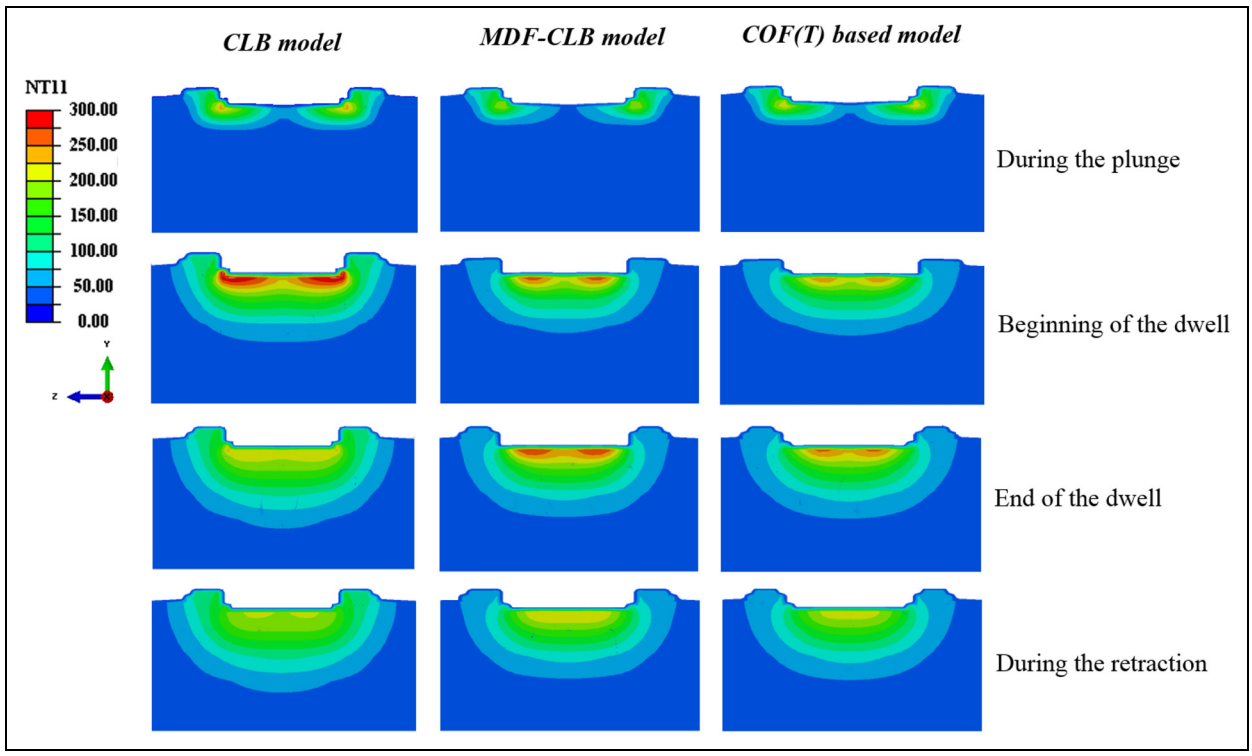

Figure 3. Comparison of simulated temperature distributions in the weld cross-section using different friction models during the different stages of FSSW process.

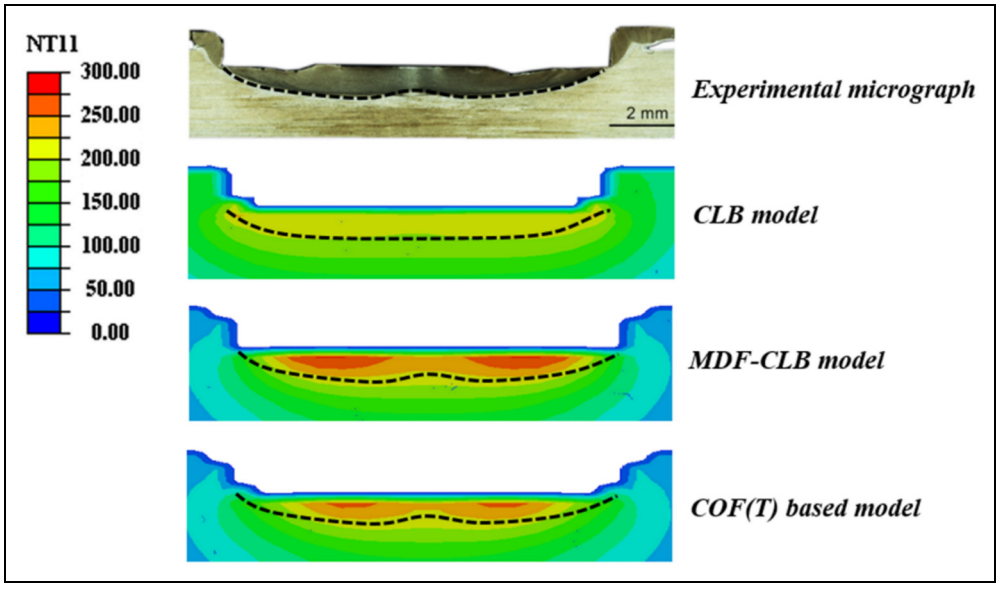

Figure 4. Comparison between simulated temperature distribution by the end of the dwelling stage and experimental micrograph in the weld cross-section.

combined effect of heat generation and dissipation during FSSW. The heat is generated through two different thermo-mechanical mechanisms, namely the friction work and the plastic deformation work. According to the numerical results, the highest temperature zone is located right below the tool, but away from the weld centre. This result could be attributed to the use of a pinless tool with a flat shoulder. The absence of the pin stirring action results in reduced material flow in the weld centre, which leads to a decrease in the heat generated from plastic deformation work.

To illustrate this interpretation, Figure 5 displays the equivalent plastic strain distribution in the radial direction at the top surface of the workpiece for all the numerical simulations. A simple visual inspection of the curves reveals that the shape of the equivalent plastic strain

distribution is similar when using different friction models. The highest deformation values are always registered near the tool edge and become extremely low toward the centre. However, a significant difference in the peak equivalent plastic strain is observed for the CLB model, which may explain the difference in the maximum temperature reached with this model.

Previous results showed that the temperature evolution during the simulation of FSSW was deeply influenced by the friction model. However, the mechanisms behind this evolution require further investigation. Therefore, in subsequent sections, we will focus on the study of the contribution of the energies dissipated by friction and plastic deformation on the heat generation.

Maximum temperature evolution with dissipated energy

As mentioned earlier, in FSSW the temperature evolution is highly sensitive to the amount of heat generated through two distinct mechanisms: the friction work between the contact surfaces (sliding condition) and the plastic deformation of the workpiece material (sticking condition).[24] In this section, the contact developed during welding will be assessed by evaluating the friction and plastic dissipated energies. Figure 6 shows the numerical results of the peak temperature evolution, with the dissipated energies, for the different friction models. The different stages of the FSSW process are identified in each graph. It can be seen that the predicted maximum temperature and energy dissipation are dependent on the used friction model. Thus, the effect of each friction model on the numerical results is discussed in the following.

The conventional Coulomb model (CLB). When the CLB model was used (Figure 6(a)), during the plunging stage, the temperature reached a maximum value of 200 °C, when the plastic and frictional dissipated energies attained the maximum values of 75 J and 5 J, respectively. At the beginning of the dwell, the peak temperature increased continuously with the plastic dissipated energy, meanwhile, the frictional dissipated energy remained in very low values. This feature reflects that the full sticking condition was developed at the contact interface. After a lapse of time, the temperature remained almost constant, despite the increase of the plastic dissipated energy. This result is attributed to the heat conduction transfer throughout the workpiece. In fact, with the welding time, the generated heat was spread toward the bottom surface of the workpiece. At the end of the dwelling stage, the plastic dissipated energy tended to stabilize, while a slight increase in the frictional dissipated energy took place. This indicated the beginning of sliding at the contact interface ($\boldsymbol{\tau_{crit}} = 0.3\,\sigma_N$). However, the value of the peak temperature started to decrease. This result allows deducing that the temperature evolution during the process was highly dependent on the plastic dissipated energy.

The modified Coulomb model (MDF-CLB). Addressing the results relative to the MDF-CLB model (Figure 6(b)), from a general point of view, it is possible to conclude that an important amount of frictional energy is dissipated when compared to the CLB model. This result indicates the presence of the sliding condition in some regions at the contact interface due to the introduction of the limit shear stress value of the base material. During the plunging period, the amount of the plastic dissipated energy was still higher than that of the frictional dissipated energy. It indicated the predominance of the sticking condition with the downward motion of the tool. At this stage, 110 °C maximum temperature was reached, when the attained plastic and frictional dissipated energies were 58 J and 12 J, respectively.

It can be noted that, compared to the CLB model, the small decrease in the plastic dissipated energy induced a sharp decrease in the maximum temperature, regardless of the increase of the frictional dissipated energy. When the plastic heat generation was localized near the top surface of the workpiece, the plastic deformation is likely the determinant factor for the temperature evolution, mainly during the plunging. Once the dwelling stage starts, the temperature increases slowly. It is clear that the plastic dissipated energy was steady, meanwhile, the frictional dissipated energy was increasing. The maximum temperature value reached at the end of the plunge stage is still insufficient for softening the workpiece. Therefore, with the lack of tight contact between the tool and the workpiece, the plastic deformation will be trivial and the sliding condition will prevail over the sticking one. After some time, when the temperature exceeded the value of 150 °C (softening temperature), the material of the workpiece has experienced excessive plastic deformation (Figure 2), which induced a significant rise in the plastic dissipated energy. Thereby, both energy components have started increasing at the same rate, which indicates that mixed sliding-sticking conditions were developed.

The temperature-dependent friction coefficient-based model (COF (T)). Figure 6(c) shows the evolution of temperature and frictional and plastic dissipated energies for the COF(T) based model. It is noted the important contributions of both dissipated energies in the heat generation. It also indicates the presence of mixed sliding-sticking contact conditions. However, compared to the MDF-CLB model, a higher temperature was reached at the end of the plunge (165 °C), when the plastic and frictional dissipated energies were 69 J and 9 J, respectively. It is also obvious to note that the increase in the temperature was caused by the rise in the energy dissipated from the plastic deformation work. During the dwelling period, a sharp decrease in the rate of plastic dissipated energy was observed, contrary to the frictional dissipated energy which was increased most rapidly. Similar to the two previous models, the reduction in the tool pressure after the transition from the plunging to the dwelling

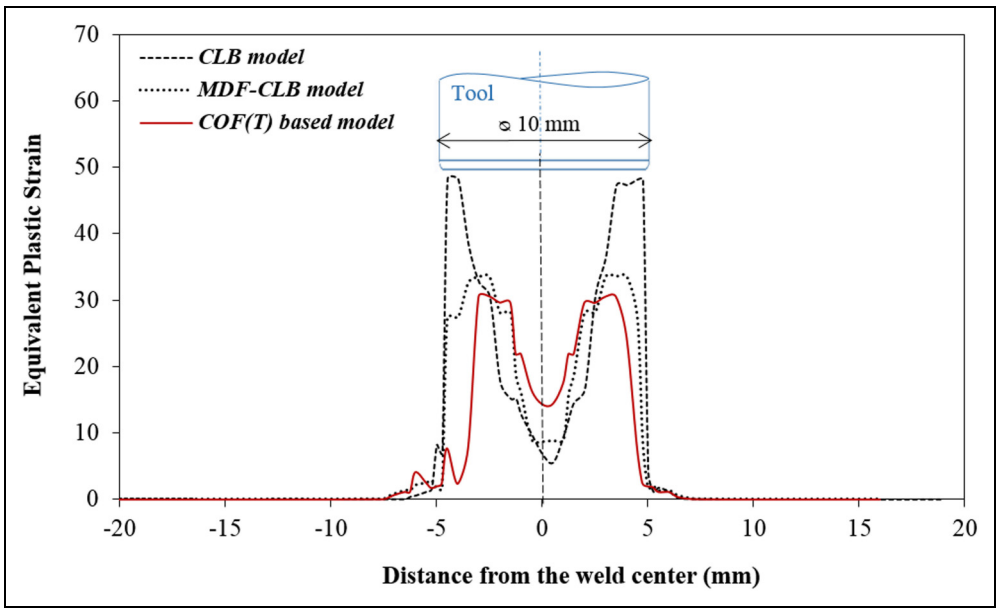

Figure 5. Plots of equivalent plastic strain versus distance away from the tool centre for the different friction models.

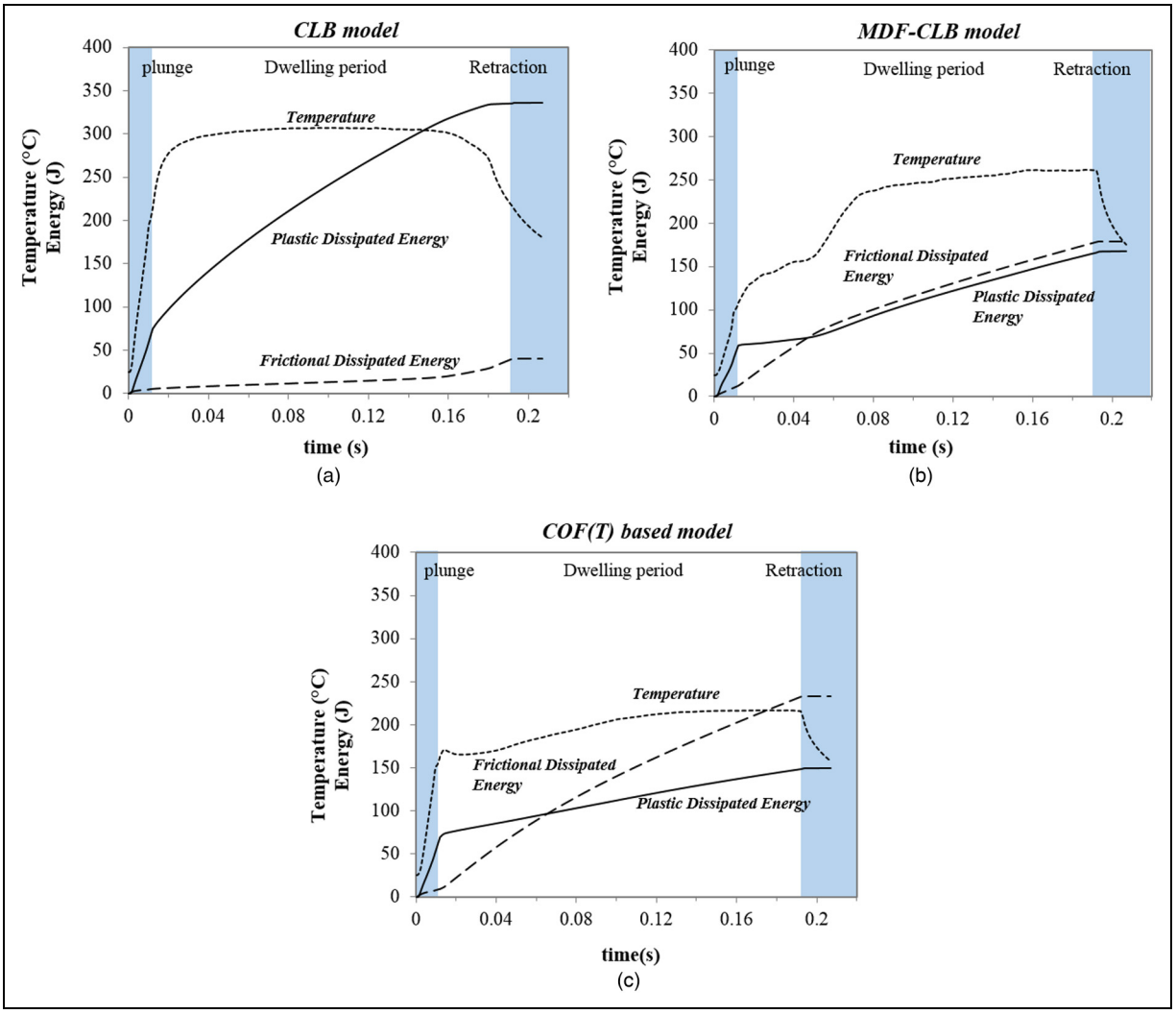

Figure 6. Temperature evolution with dissipated energy for different friction models: (a) CLB model; (b) MDF-CLB model; (c) COF(T) model.

stage induced a decrease in the plastic deformation along the thickness direction. Contrary to the MDF-CLB model, the plastic dissipated energy in this case, continued to increase from the beginning of the dwelling stage. According to Figure 2, the temperature value of 165 °C, reached at the end of the plunge stage was high enough to cause softening within the weld zone.

The maximum stabilized temperature, predicted using the COF (T) based model, was lowest than that forecasted using the other models. In fact, when using the temperature-dependent-COF based model, different values of critical shear stress were considered according to the temperature reached at the contact interface. This fact allows the sliding condition to overcome the sticking one, which is reflected by the high amount of the frictional dissipated energy during the process. Moreover, as presented in Table 2, the values of COF given by Meyghani et al.[22] were lower than 0.3 (introduced in the CLB and the MDF-CLB models), which leads to an earlier transition from the sticking to the sliding state. These findings for the COF (T) based model are consistent with Su et al.[38] works. It was stated, based on an analytical study for the FSSW process, that almost the whole mechanical energy was converted into viscous heat. Schmidt & Hattel[33] drew similar conclusions, assuming that the sticking condition predominated during welding. Thus, the heat generation at the tool-workpiece interface was primarily caused by plastic dissipation energy. Similar conclusions, regarding the heat generation proportions, were reported by Li et al.[31] The authors claimed that the heat generation during FSW depends on the intense plastic deformation of the thin shear layer at the tool-workpiece interface.

It should also be noted that, for all the friction models, a steady-state of the dissipated energies during the retraction stage is explained by the fact that the energy extracted from ABAQUS© is a cumulative result (history output). Therefore, when there is no energy source, the dissipated energies remain constant.

Numerical versus experimental results

The analysis performed in the previous item showed the contact conditions prescribed according to the different friction models, as well as the temperature evolution during welding. The predicted temperature evolution was compared to the experimental results, to examine the accuracy of each friction model. Figure 7 shows the predicted and experimental maximum temperature evolution. One can observe that the numerical simulation performed using the COF (T) based model is in good agreement with the experimental measurements.

Compared with experimental results, the thermal cycle obtained using the CLB model displays a maximal average relative error of 50% (about 100 °C). This result disproves the assumption of 0.3 as a COF value for the present process conditions. According to Dixit et al.[39] any friction model can be linearized in the form of a CLB model for a very narrow load range; but further

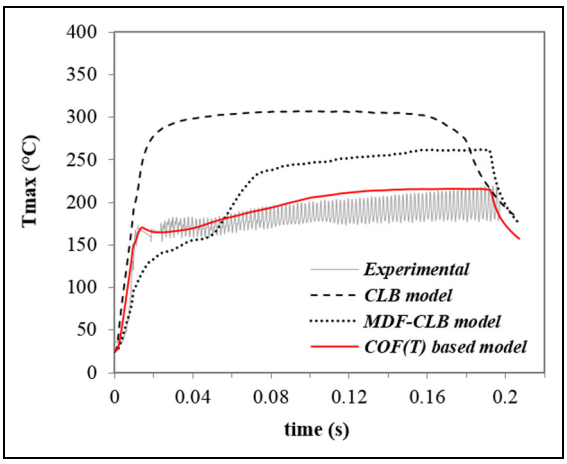

Figure 7. Comparison of the maximum temperature evolution using different friction models with experimental results.

than a certain load, the COF decreases along with the normal pressure. This statement may explain the very large differences in the predicted temperature between the CLB model and the experimental results. Therefore, one should be aware in the selection of the COF when using the CLB model.

For the MDF-CLB model, the difference between the numerical and the experimental results decreases, reaching an average relative error of about 25% during the dwell period. It is important to stress that, during the plunge period until the beginning of the dwelling stage, the model underestimates the welding temperature. However, during the dwell stage, the model overestimates the temperature, once the plastic dissipated energy starts to increase. These results indicate the weakness of MDF-CLB models, mainly when the material exhibits large plastic deformation. It is also important to mention that the yield shear stress (τ_{yield}) of the material during welding depends on the temperature. However, the evolution of τ_{yield} with the temperature is not considered when defining the MDF-CLB model under ABAQUS©. This was one of the software limitations. Despite the limitation of the conventional and the modified versions of the Coulomb model in the rational description of friction in the numerical simulation of FSSW process, they are the most used in literature. Contrary, we showed that the COF (T) based model predicts high accurate results compared to those obtained using CLB or MDF-CLB models in the simulation of FSSW process. From this comparison, it can be deduced that the friction coefficient evolution with temperature (Table 2) reflects the real effect of the material softening on the contact state during FSSW. This result was endorsed by Moore & Tegart[40] who claimed that the coefficient of friction decreases with the yield pressure.

In order to improve the accuracy of the CLB and MDF-CLB friction models in the prediction of the welding temperatures, a simple approach was experienced. More precisely, the constant COF, for both models, was adjusted to a lower value ($\mu = 0.23$). The

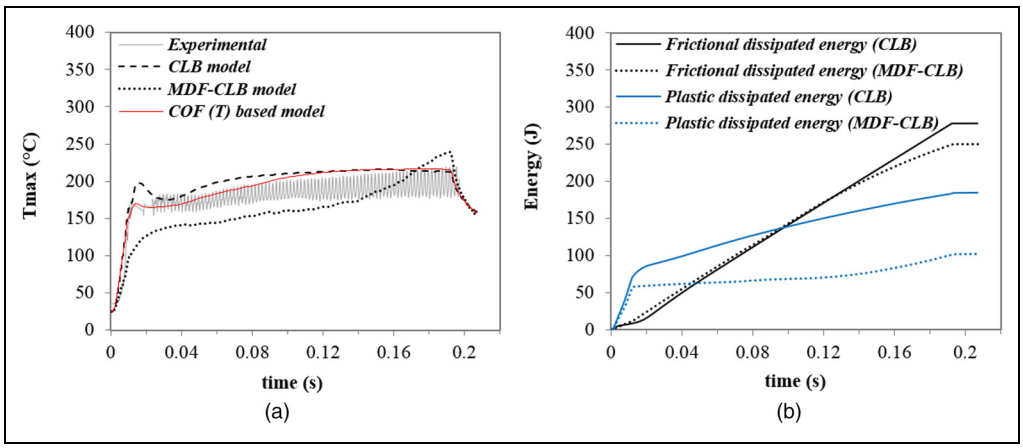

Figure 8. Numerical results obtained with CLB model and MDF-CLB model when using a COF = 0.23: (a) The maximum temperature evolution; (b) frictional and plastic dissipation energies.

new results of maximum temperature evolution are plotted in Figure 8(a). The comparison between the computed and experimentally obtained results shows a clear improvement in the predictive capability of both friction models.

Figure 8 displays the results of the frictional and plastic dissipated energies using the friction coefficient of 0.23. Compared to the results presented in Figure 6(a) and (b), a significant decrease in the amount of plastic dissipated energy is detected. Meanwhile, the frictional dissipated energy exhibits a significant increase. This result reflects the earlier occurrence of the sliding condition when reducing the COF value. According to Mekote et al.[41] the apparent friction coefficient measured using tribometers is often overestimated, because they did not consider the intense contact pressure and the plastic deformation that were taking place during welding. Moreover, depending on the relative motion of the contact surfaces, two types of friction may occur: kinetic friction associated with a linear motion, and rolling friction associated with rotational motion. The coefficient of rolling friction is generally smaller than the kinetic friction coefficient.[42] Therefore, to improve accuracy in the FSSW simulation, the contact model should involve the component of the rolling friction; thus a reduced value of the COF is to be considered. Nevertheless, the effect of temperature on the friction coefficient should also be taken into account. Consequently, an accurate prediction and a better comparison with experimental results could be achieved.

Conclusions

This work puts forward a thorough analysis of the effect of three friction models on the heat generation sources (i.e. energy dissipation by friction and plastic deformation) and the temperature evolution in the FSSW process simulation. A 3D thermo-mechanical FE analysis, using three different friction models, namely, the conventional Coulomb model (CLB), the modified Coulomb model (MDF-CLB), and the temperature-dependent friction coefficient-based model (COF(T)), was performed for the AA6082-T6 aluminium alloy. For each friction model, the amount of energies dissipated by friction and by the plastic deformation along with their contribution to the maximum temperature evolution were calculated. Then, the comparison between prediction of the models and the experiments was established. Based on this analysis, the following conclusions can be drawn:

- For the AA6082-T6 aluminium alloy, which exhibits large plastic deformation during welding, the plastic dissipated energy was the main source of heat generation and subsequently the determining factor in the evolution of temperature during the process.
- During the FSSW process, the predominance of a contact condition, whether sliding or sticking, affects the amount of heat generation from both friction work and plastic deformation. Therefore, the friction models parameters, mainly, the friction coefficient (COF) and the material yield shear stress (τ_{yield}), which determine the transition from the sticking to sliding condition, need to be fine-tuned.
- When using the CLB and the MDF-CLB friction models, the constant values of COF and τ_{yield} should consider the high contact pressure and the severe material plastic deformation. The experimentally measured COFs are often overestimated, and reduced values need to be introduced for more reliable numerical simulations.
- The COF(T) based model, which considers the material softening at high temperature, was found to be the most suitable friction model to predict the real temperature evolution during the FSSW of AA6082-T6 aluminium alloy.

These findings clearly demonstrated that an efficient numerical analysis of FSSW may be achieved when considering the material behaviour in the selection of the friction models parameters. This approach could eventually

lead to an efficient contact modelling strategy for the numerical simulation of the FSSW and the FSW processes.

Acknowledgements

This work was supported by FEDER funds through COMPETE – Programa Operacional Factores de Competitividade –, and by FCT – Fundação para a Ciência e a Tecnologia, under the R&D Unit Institute for Sustainability and Innovation in Structural Engineering (ISISE), under reference UIDB/04029/2020; Centre for Mechanical Engineering, Materials and Processes (CEMMPRE), under reference UIDB/00285/2020; and by the project Friction 4.0 (POCI-01-0145-FEDER-032089). The co-author A. Khalfallah gratefully acknowledge his support by FEDER funds through the programme COMPETE and by national funds through FCT, under the project UID/EMS/00285/2020. He was also supported by the project RDFORMING (reference PTDC/EMEEME/31243/2017), co-funded by FCT, and by FEDER, through the programme Portugal-2020 (PT2020), and by POCI, with reference POCI-01-0145-FEDER- 031243. All supports are gratefully acknowledged.

Authors' contributions

Nasra Hannachi: Investigation, Software, Data curation, Formal analysis, Writing – original draft, Writing – review & editing. Ali Khalfallah: Conceptualization, Methodology, Writing – review and editing, Supervision. Carlos Leitão: Methodology, Investigation, Data curation, Writing – review & editing. Dulce Rodrigues: Conceptualization, Methodology, Writing – review and editing, Supervision.

Declaration of conflicting interests

The authors declared no potential conflicts of interest with respect to the research, authorship, and/or publication of this article.

Funding

The authors received no financial support for the research, authorship and/or publication of this article.

ORCID iDs

Nasra Hannachi https://orcid.org/0000-0003-0053-796X
Ali Khalfallah https://orcid.org/0000-0002-3234-8795
Carlos Leitão https://orcid.org/0000-0003-0181-7146

References

1. Yang XW, Fu T and Li WY. Friction stir spot welding: a review on joint macro- and microstructure, property, and process modelling. *Adv Mater Sci Eng* 2014; 2014: 11. Article ID 697170. Epub ahead of print 2014. DOI: 10.1155/2014/697170.
2. Arul SG, Pan T, Lin PC, et al. Microstructures and failure mechanisms of spot friction welds in lap-shear specimens of aluminum 5754 sheets. *SAE World Congr* 2005; Technical Paper. No 2005-01-1256. 2005. DOI: 10.4271/2005-01-1256.
3. Awang M, Mucino VH, Feng Z, et al. Thermo-mechanical modeling of friction stir spot welding (FSSW) process: use of an explicit adaptive meshing scheme. *SAE World Congr* 2005; Technical Paper No 2005-01-1251. DOI: 10.4271/2005-01-1251.
4. Cederqvist L and Reynolds AP. Factors affecting the properties of friction stir welded aluminum lap joints. *Weld J (Miami, Fla)* 2001; 80: 281–287.
5. Muci-Küchler KH, Kakarla SST, Arbegast WJ, et al. Numerical simulation of the friction stir spot welding process. *SAE World Congr* 2005; Technical Paper No 2005-01-1260.
6. Muci-Küchler KH, Kalagara S and Arbegast WJ. Simulation of a refill friction stir spot welding process using a fully coupled thermo-mechanical FEM model. *J Manuf Sci Eng* 2010; 132: 014503-014503-5. Epub ahead of print 2010. DOI: 10.1115/1.4000881.
7. Malik V, Sanjeev NK, Hebbar HS, et al. Investigations on the effect of various tool pin profiles in friction stir welding using finite element simulations. *Procedia Eng* 2014; 97: 1060–1068.
8. Chen LX and Ni J. Thermal-mechanical modeling on friction stir spot welding of dissimilar materials based on Coupled Eulerian-Lagrangian approach. *Int J Adv Manuf Technol* 2017; 91: 1697–1707.
9. Ansari MA and Behnagh RA. Numerical study of friction stir welding (FSW) plunging phase using smoothed particle hydrodynamics (SPH). *Model Simul Mater Sci Eng* 2019; 27: 055006 1697-1707.
10. Guerdoux S, Fourment L, Miles M, et al. Numerical simulation of the Friction Stir Welding Process using both Lagrangian and Arbitrary Lagrangian Eulerian formulations. In: Materials processing and design: modeling, simulation and applications, NUMIFORM 2004 conference proceeding, 2004.
11. Sanjeev and Ravikiran. Application of coupled Eulerian Lagrangian approach in finite element simulation of friction stir welding. In: Simulia community conference proceedings 2015, 2015.
12. Pan W, Li D, Tartakovsky AM, et al. A new smoothed particle hydrodynamics non-Newtonian model for friction stir welding: process modeling and simulation of microstructure evolution in a magnesium alloy. *Int J Plast* 2013; 48: 189–204.
13. Jedrasiak P and Shercliff HR. Small strain finite element modelling of friction stir spot welding of Al and Mg alloys. *J Mater Process Technol* 2019; 263: 207–222.
14. Bagheri B, Abbasi M and Hamzeloo R. The investigation into vibration effect on microstructure and mechanical characteristics of friction stir spot vibration welded aluminum: simulation and experiment. *Proc Inst Mech Eng Part C J Mech Eng Sci* 2020; 234: 1809–1822.
15. Lorrain O, Zahrouni H and El Hadrouz M. A contribution to a critical review of friction stir welding numerical simulation. *J Mech Mater Struct* 2009; 4: 351–369.
16. Chiumenti M, Cervera M, Agelet de Saracibar C, et al. Numerical modeling of friction stir welding processes. *Comput Methods Appl Mech Eng* 2013; 254: 353–369.
17. Andrade DG, Leitão C, Dialami N, et al. Analysis of contact conditions and its influence on strain rate and temperature in friction stir welding. *Int J Mech Sci* 2021; 191: 386–474. Epub ahead of print 2021. DOI: 10.1016/j.ijmecsci.2020.106095.
18. Frigaard Grong and Midling OT. A process model for friction stir welding of age hardening aluminum alloys. *Metall Mater Trans A* 2001; 32: 1189–1200.
19. D'Urso G. Thermo-mechanical characterization of friction stir spot welded AA6060 sheets: experimental and FEM analysis. *J Manuf Process* 2015; 17: 108–119.

20. Yang X, Feng W, Li W, et al. Numerical modelling and experimental investigation of thermal and material flow in probeless friction stir spot welding process of Al 2198-T8. *Sci Technol Weld Join* 2018; 23: 704–714.
21. Khosa SU, Weinberger T and Enzinger N. Thermo-mechanical investigations during friction stir spot welding (FSSW) of AA6082-T6. *Weld World* 2010; 54: R134–R146. Epub ahead of print 2010. DOI: 10.1007/BF03263499.
22. Meyghani B and Awang M. Developing a finite element model for thermal analysis of friction stir welding (FSW) using hyperworks. In: *Advances in Material Sciences and Engineering*, Singapore. 2020; 619–628. DOI: 10.1007/978-981-13-8297-0_64.
23. Zhang Z and Chen JT. The simulation of material behaviors in friction stir welding process by using rate-dependent constitutive model. *J Mater Sci* 2008; 43: 222–232.
24. Dialami N, Chiumenti M, Cervera M, et al. Enhanced friction model for friction stir welding (FSW) analysis: simulation and experimental validation. *Int J Mech Sci* 2017; 133: 555–567.
25. Cervera M, De Saracibar CA and Chiumenti M. COMET – A Coupled Mechanical and Thermal Analysis Code. Data Input Manual. Version 5.0. 2002. Epub ahead of print 2002. DOI: 10.1063/1.3457640.
26. Costa MI, Leitão C and Rodrigues DM. Parametric study of friction stir welding induced distortion in thin aluminium alloy plates: a coupled numerical and experimental analysis. *Thin Walled Struct* 2019; 134: 268–276.
27. Abaqus. Abaqus v.6.14 user's manual, dassault systemes simulia corporation. Providence, RI, USA., 2014.
28. Sabari S, Galvão I, Leitão C, et al. Influence of softening mechanisms on base materials plastic behaviour and defects formation in friction stir lap welding. *J Manuf Mater Process* 2020; 4(4). Epub ahead of print 2020. DOI: 10.3390/jmmp4040120.
29. Leitão C, Louro R and Rodrigues DM. Analysis of high temperature plastic behaviour and its relation with weldability in friction stir welding for aluminium alloys AA5083-H111 and AA6082-T6. *Mater Des* 2012; 37: 402–409.
30. Summers PT, Chen Y, Rippe CM, et al. Overview of aluminum alloy mechanical properties during and after fires. *Fire Sci Rev*. 2015; 4: 1–36. DOI: 10.1186/s40038-015-0007-5.
31. Li W, Zhang Z, Li J, et al. Numerical analysis of joint temperature evolution during friction stir welding based on sticking contact. *J Mater Eng Perform* 2012; 21: 1849–1856.
32. Li W, Shi S, Wang F, et al. Numerical simulation of friction welding processes based on ABAQUS environment. *J Eng Sci Technol Rev* 2012; 5: 10–19.
33. Schmidt H and Hattel J. A local model for the thermomechanical conditions in friction stir welding. *Model Simul Mater Sci Eng* 2005; 13: 77–93.
34. Zhang Z and Zhang HW. Numerical studies on controlling of process parameters in friction stir welding. *J Mater Process Technol* 2008; 9: 241–270.
35. Hamilton R, Mackenzie D, Li H, et al. Multi-physics simulation of friction stir welding process. *Int J Comput Aided Eng Softw* 2010; 27: 967–985.
36. Jedrasiak P, Shercliff HR, Reilly A, et al. Thermal modeling of Al-Al and Al-steel friction stir spot welding. *J Mater Eng Perform* 2016; 25: 4089–4098.
37. Andrade DG, Leitão C and Rodrigues DM. Influence of base material characteristics and process parameters on frictional heat generation during friction stir spot welding of steels. *J Manuf Process* 2019; 43: 98–104.
38. Su P, Gerlich A, North TH, et al. Energy utilisation and generation during friction stir spot welding. *Sci Technol Weld Join* 2006; 11: 163–169.
39. Dixit US, Yadav V, Pandey PM, et al. Modeling of friction in manufacturing processes. In: *Mechanics of Advanced Materials edited by P.T. Silberschmidt*. Elsevier 2020; 415–444.
40. Moore AJ and Tegart WJ (1952). Relation between friction and hardness. Proc R Soc London Ser A 1952; 212: 452–458.
41. Melkote SN, Grzesik W, Outeiro J, et al. Advances in material and friction data for modelling of metal machining. *CIRP Ann - Manuf Technol* 2017; 66: 731–754.
42. Awang M. *Simulation of friction stir spot welding (FSSW) process: study of friction phenomena*. PhD Thesis, West Virginia University, West Virginia, 2007.